Provenance ages of late Paleozoic sandstones (Santa Rosa Formation) from the Maya block, SE Mexico. Implications on the tectonic evolution of western Pangea

Bodo Weber[1,*], Peter Schaaf[2], Victor A. Valencia[3], Alexander Iriondo[4], and Fernando Ortega-Gutiérrez[2]

[1] *División Ciencias de la Tierra, Centro de Investigación Científica y de Educación Superior de Ensenada (CICESE), Km. 107 carretera Tijuana-Ensenada, 22860 Ensenada BC, Mexico.*
[2] *Instituto de Geofísica, Instituto de Geología, Universidad Nacional Autónoma de México, Ciudad Universitaria, Delegación Coyoacán, 04510 México D.F., Mexico.*
[3] *Department of Geosciences, University of Arizona, 1040 East Fourth St., Tucson AZ, 85721-0077 U.S.A.*
[4] *Centro de Geociencias, Universidad Nacional Autónoma de México, Campus Juriquilla, 76230 Querétaro, Mexico. and Department of Geological Sciences, University of Colorado at Boulder, Boulder CO, 80309 U.S.A.*
* bweber@cicese.mx

ABSTRACT

The Santa Rosa Formation in the State of Chiapas is a sequence of flysch-type sediments of Mississippian to Pennsylvanian age. These sedimentary rocks correlate with the Santa Rosa Group of Guatemala and Belize and crop out along the southern limit of the Maya block north of the Motagua fault, which is currently considered the border between the North American and the Caribbean plates. Ages of individual zircon grains from sandstones of the Upper Santa Rosa Formation in southern Mexico were analyzed by Laser Ablation Multicollector ICPMS and by SHRIMP. The youngest zircon population is of Silurian age (~420 Ma), but most grains have ages that correspond to the Pan-African-Brasiliano orogenic cycle (500–700 Ma). Other minor populations have ~820 Ma, Grenville (1.0–1.3 Ga), Mesoproterozoic (1.4–1.6 Ga), Paleoproterozoic (1.8–2.2 Ga), and Archean (2.7–3.1 Ga) ages. Most of the sediments came from either present-day West Africa or NE South America, where both Pan-African-Brasiliano orogens and cratonic landmasses are present. In our model, southwestward progressive collision of Gondwana with Laurentia during the Alleghanian orogeny resulted in erosion and deposition of flysch-type sediments to the west, followed by westward movement of the Maya block and adjacent lithosphere.

Key words: provenance ages, zircon, sediments, SE Mexico, Gondwana, Pan-African-Brasiliano.

RESUMEN

La formación Santa Rosa en el estado de Chiapas es una secuencia de sedimentos tipo flysch de edad Misisípica a Pensilvánica. Estas rocas sedimentarias correlacionan con el Grupo Santa Rosa de Guatemala y de Belice y afloran a lo largo del límite sur del bloque Maya al norte de la falla Motagua, la cual se considera actualmente como el límite entre las placas de Norteamérica y del Caribe. Se analizaron edades de zircones individuales de areniscas de la Formación Santa Rosa Superior en el Sur de México por ICPMS multicolector con ablación con láser y con SHRIMP. La población más joven de zircones es de edad silúrica (~420 Ma), pero la mayoría de los zircones tiene edades que corresponden con el ciclo orogénico Pan-Africano-Brasiliano (500–700 Ma). Otras poblaciones menores tienen edades de ~820 Ma, del Grenvilleano (1.0–1.3 Ga), del Mesoproterozoico (1.4–1.6 Ga), del Paleoproterozoico (1.8–2.2

Ga) y del Arqueano (2.7–3.1 Ga). La mayoría de los sedimentos proviene del oeste de Africa o del este de Sudamérica, donde se encuentran tanto orógenos con edades del ciclo Pan-Africano-Brasiliano como cratones precámbricos. En nuestro modelo, la colisión progresiva entre Gondwana y Laurentia durante la orogenia Alleghaniana resultó en erosión y deposición de los sedimentos flyschoides hacia el oeste, seguido por un movimiento del bloque Maya y la litósfera adyacente en dirección poniente.

Palabras clave: edades de proveniencia, zircón, sedimentos, SE México, Gondwana, Pan-Africano-Brasiliano.

INTRODUCTION

Since the first reconstruction of Pangea by Bullard *et al.* (1965) with overlapping areas between South America and parts of southern Mexico, the paleogeographic position of pre-Mesozoic crustal blocks in Mexico, Central America, and the Caribbean region have been of special interest in solving the spatial problems posed by the Pangea reconstruction (Ross and Scotese, 1988; Pindell and Barrett, 1990; Pindell *et al.*, 2000). Southern Mexico and Central America consist of several blocks with different crustal evolution that are separated by major fault zones, and hence these crustal blocks were defined as tectono-stratigraphic terranes whose origin and relation to each other is uncertain (Campa and Coney, 1983; Sedlock *et al.*, 1993; Ortega-Gutiérrez *et al.*, 1994). Large scale sinistral strike-slip movements along the hypothetical Mojave-Sonora Megashear (*e.g.*, Anderson and Schmidt, 1983), the Trans-Mexican Volcanic Belt (*e.g.*, Shurbet and Cebull, 1984), and along the Motagua-Polochic fault system (*e.g.*, Anderson and Schmidt, 1983; Burkart and Self, 1985) have been assumed to accommodate the Mexican terranes and the Chortís block of Central America prior to the opening of the Gulf of Mexico in Triassic to Jurassic times. Plate reconstructions on the basis of geological and geophysical constraints have shown that most of the Mexican terranes reached their present position with respect to Laurentia after Carboniferous times (Dickinson and Lawton, 2001). On the other hand, Precambrian (Grenville) granulite basement, the Oaxaquia micro-continent, which is thought to underlie most of central and southern Mexico (Ortega-Gutiérrez *et al.*, 1995) and a Permian magmatic arc which occur along the entire length of Mexico (Torres *et al.*, 1999), indicate that these crustal blocks were in contact at least since Permian times. The pre-Mesozoic positions of all these land masses either as peri-Gondwanan blocks between Gondwana and Laurentia or as outboard terranes in the Pacific margin, are important for the understanding of the late Paleozoic assembly of western Pangea.

Provenance studies of zircons from late Paleozoic sedimentary rocks in southeastern Mexico provide important arguments (1) to define the paleo-positions of the crustal blocks prior to the assemblage of Pangea and (2) to test geologic relations proposed between adjacent geologic units and crustal blocks. In this paper, we present U-Pb ages of individual zircons from sandstones of the late Paleozoic Santa Rosa Superior Formation from southern Mexico, which were obtained both by SHRIMP (sensitive high-resolution ion microprobe) and LA-MC-ICPMS (laser ablation– multi-collector–inductively coupled plasma mass-spectrometer) analysis.

GEOLOGICAL BACKGROUND

Regional geology

The pre-Mesozoic basement rocks of Central America extent from the state of Chiapas in Mexico to Guatemala, Belize, and Honduras (Figure 1). The sinistral Motagua-Polochic fault system is the most important tectonic structure that crosses the entire region. This Neogene fault system is the plate boundary between the North American and Caribbean plates, continuing from the Cayman trough in the Caribbean Sea to the east into the Gulf of Tehuantepec to the west (*e.g.* Muehlberger and Ritchie, 1975; Burkart, 1983).

The Maya block (Dengo, 1985), Maya terrane (Sedlock *et al.*, 1993), or Yucatan-Chiapas block (Dickinson and Lawton, 2001) is exposed north of the Motagua fault as the southeasternmost of the Mexican terranes and includes the Yucatan peninsula, parts of the coastal plain of the Gulf of México, and southeastern México to the Tehuantepec isthmus. Pre-Mesozoic rocks crop out only in the southern part of the Maya block. East of the Tehuantepec isthmus, the Chiapas Massif extends over an area of more than 20,000 km^2 parallel to the Pacific coast (Figure 1b). It is the most voluminous of the Permian crystalline complexes in México and is composed mainly of deformed plutonic and metamorphic rocks (Damon *et al.*, 1981; Schaaf *et al.*, 2002; Weber *et al.*, 2005). Most of the metamorphic rocks in the Chiapas massif are orthogneisses; however, metasedimentary rocks crop out in several areas of the massif (Weber *et al.*, 2002). The protoliths of these metasedimentary rocks are pelitic and psammitic clastic sediments, graywackes, calcsilicates, and limestones. These sequences reached medium- to high-grade metamorphic conditions and anatexis during a late Permian orogenic event, and they were synchronously intruded by igneous rocks of the Chiapas batholith (Weber *et*
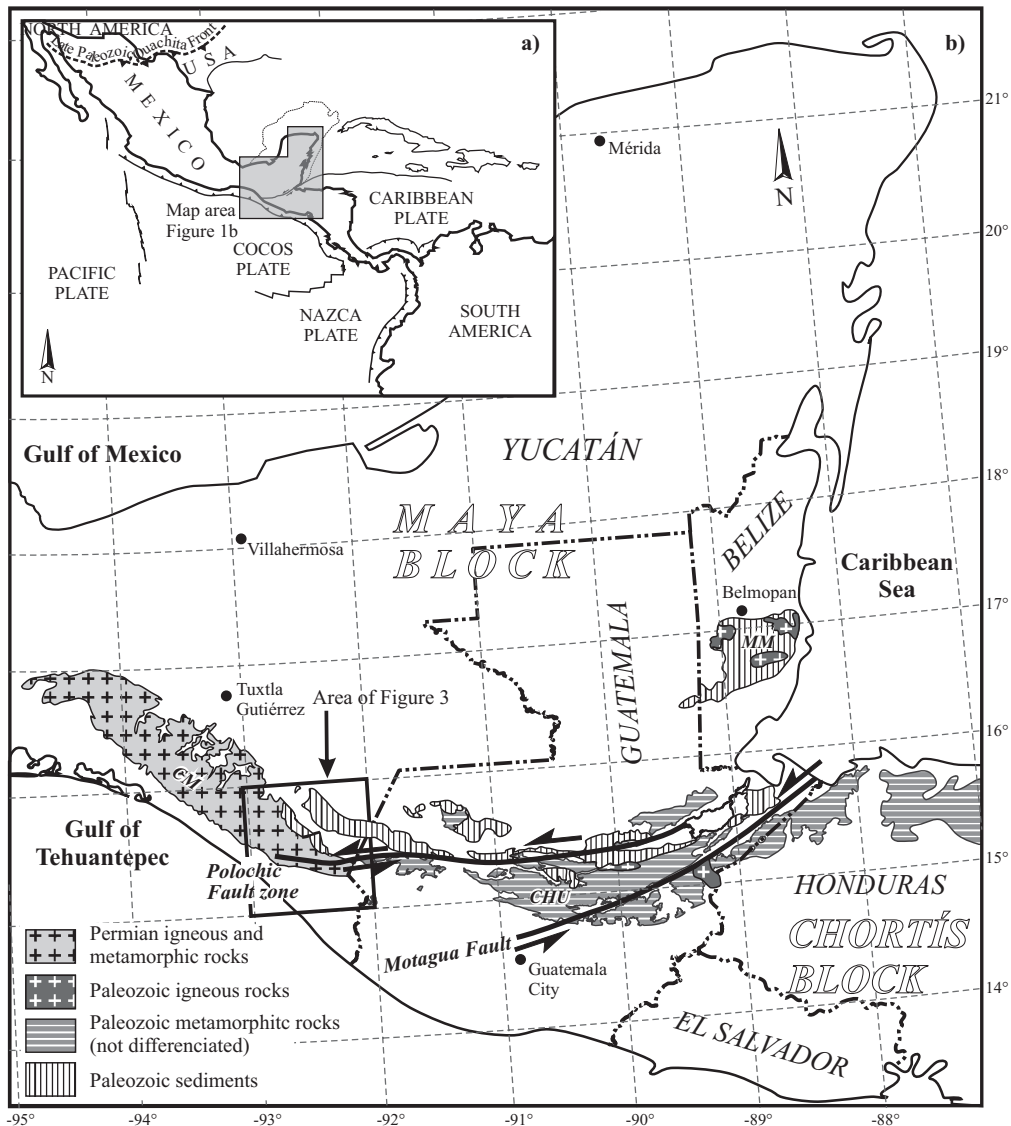
Figure 1. a: Plate-tectonic overview of Central America. b: Simplified geologic map showing pre-Mesozoic rocks exposed in southeastern México and Central America (modified after Ortega-Gutiérrez *et al.*, 1992, and French and Schenk, 1997). Abbreviations: CM: Chiapas Massif, CHU: Sierra de Chuacús, MM: Maya Mountains.

al., 2006; Hiller *et al.*, 2004). Late Paleozoic (Mississipian to Leonardian) sediments of the Santa Rosa Group crop out east of the Chiapas Massif, in the central cordillera of Guatemala, and in the Maya Mountains of Belize (Figure 1b). At least in the Maya Mountains, older sediments intruded by Silurian granites (Steiner and Walker, 1996) underlie the Santa Rosa Group. The Chuacús group (Dengo, 1985) or Chuacús complex (Ortega-Gutiérrez *et al.*, 2004) is situated between the Polochic and the Motagua faults in central Guatemala (Figure 1b) and contains Paleozoic medium- to high-grade metamorphic rocks with eclogitic relics. Dengo (1985) correlated the Chuacús complex with metasediments from the Chiapas Massif, and thus the Chuacús complex was considered as belonging to the Maya block. However, recent studies suggested that the Chuacús complex is possibly an

independent fault-bounded terrane between the Maya and the Chortís blocks (Ortega-Gutierrez *et al.*, 2004).

The Chortís block is located south of the Motagua fault and includes southern Guatemala, El Salvador, Honduras, and most of Nicaragua (*e.g.*, Dengo, 1985 and references therein). The Chortís block does not contain unmetamorphosed Paleozoic rocks like the Maya block. Immediately south of the Motagua fault zone, amphibolite-facies rocks and migmatites of the Las Ovejas complex represent the basement of the Chortís block in southern Guatemala. The most extensive sequence in the Chortís block of possible Paleozoic age is composed of low-grade metasedimentary rocks that were tentatively correlated with the Santa Rosa Group by Clemons (1966). However, a correlation of the different basement units throughout the block seems to be

problematic (Donelly *et al.*, 1990). The metamorphic basement of the Chortís block is overlain by a thick sequence of Mesozoic sedimentary rocks, somewhat different from the Mesozoic sequence in the Maya block (*e.g.*, Dengo, 1985, and references therein).

The Santa Rosa Group

The name "Santa Rosa" was first applied by Dollfus and Montserrat (1868) to clastic sedimentary rocks with interbedded limestones exposed in western Guatemala. Sapper (1937) applied the name "Santa Rosa" to a sequence of Carboniferous shales with intercalated limestone in central and western Guatemala. The original type locality (village of Santa Rosa, Baja Verapaz, Guatemala) was later demonstrated as being correlative with the Todos Santos Formation of Jurassic age (Vinson, 1962). In order to avoid confusion because of its absence at the type locality of Santa Rosa, the most abundant Upper Paleozoic shale sequence was renamed as Tactic Formation (Walper, 1960). This shale sequence is transitional into overlying massive-bedded dolomites and limestones of the Permian Chochal Formation with highly fossiliferous zones of fusulinids, corals, and brachypods of Leonardian age (Roberts and Irving, 1957; Clemons and Burkart, 1971). Clemons and Burkart (1971) proposed the use of the name Santa Rosa Group, which, in western Guatemala, includes three formations (Figure 2): (1) the lower Chicol Formation exposed near Huehuetenango is a sequence of conglomerates and breccias between 800 and 1,200 m thick; (2) the middle Tactic Formation of Pennsylvanian-Permian age is the most widespread unit of Paleozoic rocks in northwestern Guatemala, mainly composed of brown to black shales, mudstone, minor siltstone and fine sandstone beds with a maximum thickness of 1,000 m; (3) the Esperanza Formation is the uppermost unit of the Santa Rosa Group in Guatemala. Fusulinids of the genus *Schwagerina* cf. *S. campenis* indicate Wolfcampanian age for these limestones with interbedded fossiliferous shales, sandstones and dolomites (Clemons and Burkart, 1971).

In Chiapas, Paleozoic sedimentary rocks correlative with the Santa Rosa Group were described from northwest and around the village of Chicomuselo (Figure 3). They constitute a thick sequence of flysch-type rocks with an estimated overall thickness of ~5,800 m (López-Ramos, 1979) that was subdivided into two major sequences, the Lower and the Upper Santa Rosa Formation (Figure 2; Hernández-García, 1973). The Lower Santa Rosa Formation is exposed east of Angel Albino Corzo (Figure 3), and is composed of metamorphosed (partly garnet-bearing) schists and phyllites with intercalated horizons of metaquartzites and a 10 m thick conglomerate (Hernández-García, 1973). Based on a fossiliferous horizon with Paleozoic crinoids and pelecypods (lamellibranchia), Hernández-García (1973) interpreted this sequence as being at least of late Mississippian age. Its lower limit is not exposed, and its upper limit is discordant

with respect to the overlying Upper Santa Rosa Formation of late Pennsylvanian age.

The Upper Santa Rosa Formation in Chiapas is best exposed in the area around Chicomuselo (Figure 3); it is a sequence of shale, slightly calcareous siltstone, and rarely sandy siltstone, which occasionally alternates with 0.5 to 1.2 m thick sandstones of yellowish brown and grayish green colors. These sediments do not contain identifiable fossils, but on the basis of their lithological similarity and stratigraphic relations they were correlated with the Tactic Formation of Guatemala (Hernández-García, 1973). North of Chicomuselo, the Upper Santa Rosa Formation is unconformably covered by siliceous shales and limestones of the Grupera Formation which contains fusulinids (*Schwagerina*) of Early Permian (Wolfcampanian) age (Hernández-García, 1973; López-Ramos, 1979). Therefore, the Grupera Formation correlates with the Esperanza Formation (Figure 2), which forms the uppermost part of the Santa Rosa Group in Guatemala. Similar to the Chochal Formation in Guatemala, fossiliferous gray limestones of Leonardian age concordantly cover the Grupera Formation. These limestones crop out extensively south and southeast of Chicomuselo and are named Paso Hondo Formation (Figures 2 and 3; Hernández-García, 1973).

The Santa Rosa Group was also correlated with the Paleozoic sediments and low-grade metasediments that form the largest part of the Maya Mountains in Belize (Figure 1b; Dixon, 1956; Bateson and Hall, 1977). Dixon (1956) defined a lower Maya Series with metamorphosed and isoclinally
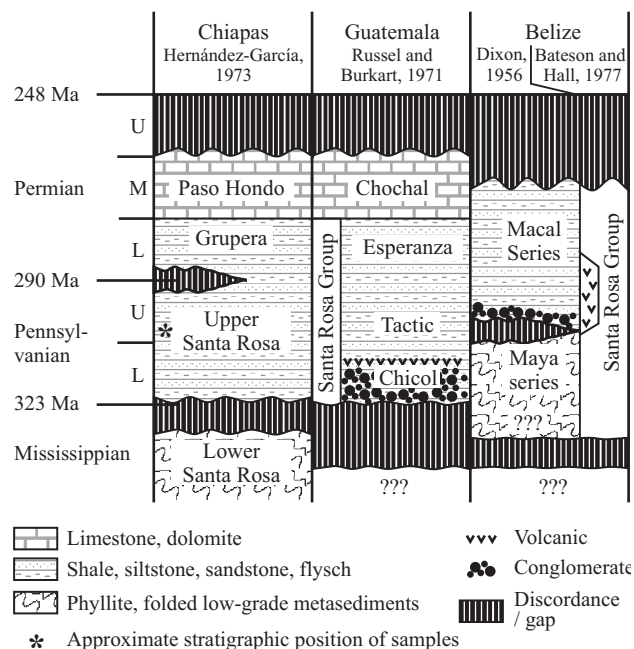
Figure 2. Comparison of the pre-Mesozoic stratigraphy of the Maya block in Chiapas after Hernández-García (1973), Guatemala after Russel and Burkart (1971), and Belize after Dixon (1956) and Bateson and Hall (1977).
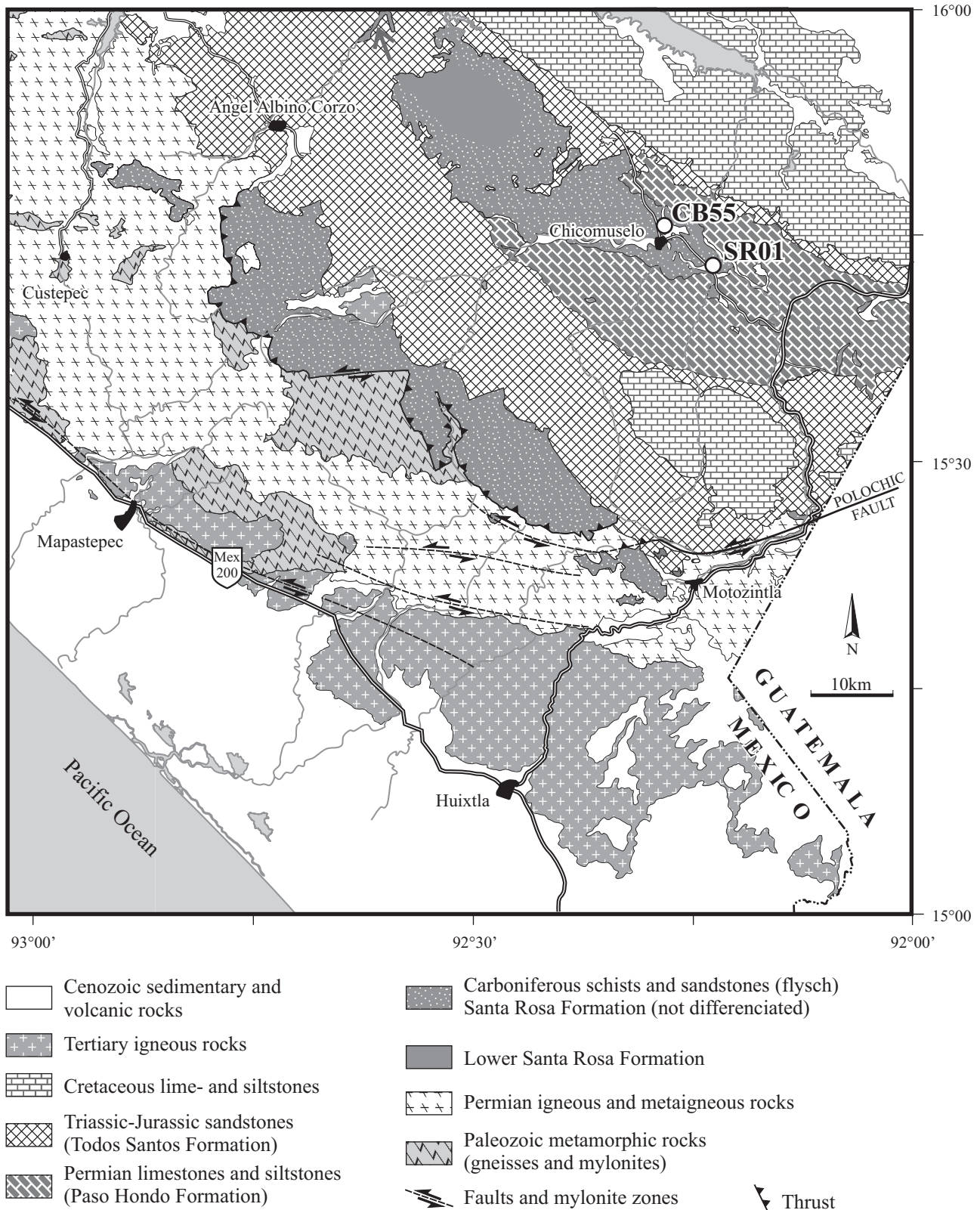
Figure 3. Simplified geologic map of eastern Chiapas (modified after the geologic map 1:250,000 Huixtla D-15-2, Jiménez-Hernández *et al.*, 2005), showing sample locations. Note: Outline of the Lower Santa Rosa Formation was inferred from a sketch map of Hernández-García (1973) and confirmed by own reconnaissance at the locality marked by grey arrow.

folded metasediments, which is discordantly overlain by the Macal series, consisting of a sequence of open-folded clastic sediments with distinctive limestone layers. (Figure 2). Bateson and Hall (1977) discarded Dixon's dichotomy and combined the Maya and the Macal series into the Santa Rosa Group with continuous sedimentation from the Pennsylvanian to the middle Permian. However, since Steiner and Walker (1996) reported Silurian crystallization ages of granites intruded into the sediments of the Maya Mountains, it seems improbable that all these sediments belong to the Santa Rosa Group. If this intrusive relation is true, Dixon's Maya Series, which do not contain fossils, might actually be of pre-Silurian age.

ANALYTICAL TECHNIQUES

Zircons were separated by standard procedures at the Geology Department at Centro de Investigación Científica y de Educación Superior de Ensenada Baja California (CICESE), and at the Instituto de Geología at Universidad Nacional Autónoma de México (UNAM), by using a Wilfley® table, a Frantz® isodynamic separator, heavy liquids, and handpicking techniques.

SHRIMP-RG

The SHRIMP procedures used in this study are similar to those reported in Nourse *et al.* (2005). Zircons handpicked from a total sample population and chips of zircon standard R33 were mounted in epoxy, ground to nearly half their thickness, and polished with 6- and 1-µm-grit diamond suspension abrasive. The mounts were cleaned in 1N HCl to avoid surface related common lead introduced to mount during polishing, and gold coated for maximum surface conductivity.

The U-Th-Pb analyses were made on 49 individual zircon grains from sample SR01 using the SHRIMP-RG (Sensitive High Resolution Ion Microprobe – Reverse Geometry) housed at Stanford University, California. The primary oxygen ion beam, operated at about 2–4 nA, excavated an area of about 25–30 µm in diameter to a depth of about 1 µm; sensitivity ranged from 5 to 30 cps per ppm Pb. Data for each spot were collected in sets of five scans through the mass range. Isotope ratios were corrected for common Pb using the measured ^{204}Pb. The reduced $^{206}Pb/^{238}U$ ratios were normalized to the zircon standard R33 which has a concordant TIMS age of 418.9 ± 0.4 Ma (2σ) (Black *et al.*, 2004). For the closest control of Pb/U ratios, one standard was analyzed after every four unknown samples. Uranium concentrations were monitored by analyzing a standard (CZ3) with ~550 ppm U. U and Pb concentrations are accurate to about 10–20%. SHRIMP isotopic data were reduced and plotted using the Squid and IsoplotEx programs of Ludwig (2001, 2003).

Laser ablation multicollector ICP-MS

LA-MC-ICPMS analyses were conducted following the method described by Dickinson and Gehrels (2003). Briefly, several hundred zircon crystals from CB-55 and fragments of a standard zircon were mounted in the inner half of the mount area. One hundred zircons were analyzed from polished section. The grains analyzed were selected at random from all of the zircons mounted. Cores of grains were preferred to avoid possible metamorphic overgrowths.

Zircon crystals were analyzed with a Micromass Isoprobe multicollector ICPMS equipped with nine Faraday collectors, an axial Daly collector, and four ion-counting channels. The Isoprobe is linked to a New Wave ArF Excimer laser ablation system, which has an emission wavelength of 193 nm. The collector configuration allows measurement of ^{204}Pb with an ion-counting channel whereas ^{206}Pb, ^{207}Pb, ^{208}Pb, ^{232}Th and ^{238}U are measured simultaneously with Faraday detectors. All analyses were conducted in static mode with a laser beam diameter of 35 µm, operated with an output energy of ~32 mJ (at 23 kV) and a pulse rate of 9 Hz. Each analysis consisted of one 20-second integration on peaks with no laser firing for backgrounds and twenty 1-second integrations on peaks with the laser firing. Hg contribution to the ^{204}Pb mass position was removed by subtracting on-peak background values. Inter-element fractionation was monitored by analyzing an in-house zircon standard which has a concordant ID-TIMS age of 564 ± 4 Ma (2σ) (Dickinson and Gehrels, 2003). This standard was analyzed once for every five unknown zircon grains. Uranium and Thorium concentrations were monitored by analyzing a standard (NIST 610 Glass) with ~500 ppm Th and U. The lead isotopic ratios were corrected for common Pb, using the measured ^{204}Pb, assuming an initial Pb composition according to Stacey and Kramers (1975) and respective uncertainties of 1.0, 0.3 and 2.0 for $^{206}Pb/^{204}Pb$, $^{207}Pb/^{204}Pb$, and $^{208}Pb/^{204}Pb$.

Systematic errors are propagated separately, and include the age of the standard, calibration correction from standard analyses, composition of common Pb, and U decay constant uncertainties. For these samples the systematic errors were 0.9 % for $^{206}Pb/^{238}U$ and 1.3 for $^{207}Pb/^{206}Pb$. The age probability plots (Ludwig, 2003) used in this study were constructed using the $^{206}Pb/^{238}U$ age for young (<0.9 Ga) zircons and the $^{207}Pb/^{206}Pb$ age for older (>0.9 Ga) grains. Interpreted ages are based on $^{206}Pb/^{238}U$ for <900 Ma grains and on $^{207}Pb/^{206}Pb$ for >900 Ma grains. This division at 900 Ma results from the increasing uncertainty of $^{206}Pb/^{238}U$ ages and the decreasing uncertainty of $^{207}Pb/^{206}Pb$ ages as a function of age. The resulting interpreted ages are shown on relative age-probability diagrams (from Ludwig, 2003). These diagrams show each age and its uncertainty (for measurement error only) as a normal distribution, and sum all ages from a sample into a single curve. All errors of both techniques are reported at the 1-σ level in Tables 1 and 2.

268 *Weber et al.*

Table 1. LA-MC-ICPMS U-Th-Pb data of detrital zircons from Santa Rosa sandstone sample CB55, Chicomuselo, Chiapas. Longitude: -92.2845°W, latitude: 15.7554°N.

Grain spot	^{206}Pb/^{204}Pb$_c$	U ppm	Th ppm	^{232}Th/^{238}U	^{207}Pb*/^{235}U ± 1σ %		^{206}Pb*/^{238}U ± 1σ %		% disc	Err corr	^{206}Pb/^{238}U (Ma) ±1σ		^{207}Pb/^{235}U (Ma) ±1σ		^{207}Pb/^{206}Pb (Ma) ±1σ	
(1)	(2)								(3)		(4)		(4)		(4)	
CB55-1	909	27	34	1.25	4.2184	5.4	0.27780	3.5	12	0.65	1580	49	1678	44	**1802**	74
CB55-3	3508	103	63	0.61	1.2906	4.9	0.13796	3.1		0.62	**833**	24	842	28	864	80
CB55-4	1025	116	106	0.91	0.6690	7.7	0.07927	0.4		0.06	**492**	2	520	31	647	166
CB55-5	948	101	75	0.74	0.3110	10.9	0.04623	2.0		0.18	**291**	6	275	26	138	255
CB55-7	11464	182	81	0.44	2.2600	0.7	0.20342	0.4	1	0.54	1194	4	1200	5	**1211**	12
CB55-8	12372	183	176	0.96	0.8306	3.0	0.10279	0.6		0.19	**631**	3	614	14	553	63
CB55-9	1677	117	100	0.85	0.8770	4.4	0.09843	2.3		0.51	**605**	13	639	21	762	80
CB55-10	7568	159	91	0.57	0.8436	3.0	0.09606	0.5		0.17	**591**	3	621	14	732	63
CB55-11	23268	407	123	0.30	1.8792	2.4	0.17539	2.3	9	0.96	1042	22	1074	16	**1139**	13
CB55-12	4124	201	117	0.58	0.7385	2.7	0.08701	0.9		0.34	**538**	5	562	12	659	54
CB55-13	3897	131	96	0.73	0.8922	4.1	0.10550	3.2		0.77	**647**	20	648	20	651	57
CB55-14	5758	61	40	0.65	7.0066	1.5	0.37768	0.8	4	0.51	2065	14	2112	13	**2158**	23
CB55-15	12770	571	306	0.54	0.5308	2.9	0.06682	0.9		0.31	**417**	4	432	10	515	60
CB55-16	821	110	36	0.33	0.8533	13.5	0.09330	1.5		0.11	**575**	8	626	64	817	285
CB55-17	5305	179	160	0.90	0.6662	4.6	0.08290	1.1		0.24	**513**	6	518	19	540	98
CB55-18	1326	92	81	0.89	0.6166	6.3	0.07466	1.5		0.23	**464**	7	488	24	600	133
CB55-19	2126	68	12	0.17	5.4783	4.0	0.31657	0.9	13	0.23	1773	14	1897	34	**2036**	69
CB55-20	5419	31	29	0.91	3.2506	4.8	0.25564	1.3	0	0.27	1467	17	1469	37	**1472**	88
CB55-21	6991	635	97	0.15	0.5776	1.8	0.07045	1.1		0.59	**439**	4	463	7	584	31
CB55-22	6096	182	157	0.87	0.7180	4.8	0.08837	1.0		0.20	**546**	5	549	20	565	103
CB55-23	1085	26	18	0.71	0.7936	12.4	0.08543	2.1		0.17	**528**	10	593	56	849	257
CB55-24	1991	77	65	0.85	0.7183	6.6	0.08682	2.8		0.42	**537**	14	550	28	604	130
CB55-26	1984	211	37	0.18	0.9403	2.9	0.11618	0.4		0.14	**709**	3	673	14	556	62
CB55-27	2074	160	107	0.67	0.7909	4.5	0.09703	1.2		0.26	**597**	7	592	20	571	95
CB55-28	3223	232	186	0.80	0.6677	2.1	0.08398	0.5		0.23	**520**	2	519	9	517	46
CB55-29	6708	275	140	0.51	0.8047	2.5	0.10138	1.2		0.48	**623**	7	599	12	513	49
CB55-30	2662	113	91	0.81	0.7500	4.6	0.08886	1.1		0.24	**549**	6	568	20	647	97
CB55-31	22353	431	160	0.37	13.5601	2.8	0.41523	2.4	28	0.89	2239	46	2719	26	**3099**	20
CB55-32	7621	136	54	0.40	3.0221	1.4	0.24695	0.4	-2	0.29	1423	5	1413	11	**1399**	26
CB55-33	3250	314	282	0.90	0.8626	2.5	0.10686	1.4		0.57	**654**	9	632	12	550	44
CB55-34	2926	228	129	0.56	0.4769	4.4	0.06620	1.0		0.23	**413**	4	396	14	296	97
CB55-35	1546	44	34	0.77	0.6576	15.0	0.09713	2.3		0.15	**598**	13	513	61	153	355
CB55-36	2575	300	174	0.58	0.6418	2.4	0.08250	1.5		0.64	**511**	7	503	9	469	40
CB55-37	698	102	75	0.73	0.7092	8.8	0.09574	0.8		0.09	**589**	4	544	37	359	200
CB55-38	1708	141	101	0.72	0.7252	4.6	0.08885	1.1		0.24	**549**	6	554	20	574	98
CB55-39	4092	301	189	0.63	0.8776	2.1	0.10752	0.4		0.19	**658**	2	640	10	574	45
CB55-40	2143	284	75	0.27	0.6692	3.3	0.08196	1.2		0.35	**508**	6	520	13	575	67
CB55-41	5435	254	68	0.27	0.6938	3.6	0.08515	0.6		0.17	**527**	3	535	15	571	78
CB55-42	1944	146	53	0.37	1.5506	1.7	0.16034	0.6	-3	0.36	**959**	6	951	11	**932**	34
CB55-43	1698	150	81	0.54	1.1464	2.2	0.12929	0.5		0.21	**784**	3	776	12	752	46
CB55-44	712	61	73	1.19	0.7350	12.6	0.08846	1.3		0.10	**546**	7	559	54	613	275
CB55-45	1075	100	103	1.03	0.3014	11.9	0.04964	0.7		0.06	**312**	2	267	28	-109	295
CB55-46	3113	58	37	0.64	1.9838	4.4	0.18658	1.4	2	0.33	1103	14	1110	29	**1124**	82
CB55-47	8311	249	30	0.12	0.8791	2.3	0.10395	0.6		0.27	**638**	4	640	11	651	48
CB55-49	2795	93	37	0.40	1.2748	2.9	0.13275	1.2		0.43	**804**	9	835	16	918	53
CB55-50	14950	281	184	0.65	0.8167	2.7	0.09639	1.4		0.53	**593**	8	606	12	655	49
CB55-51	830	30	14	0.45	0.8330	12.9	0.10140	1.7		0.13	**623**	10	615	60	588	282
CB55-54	3887	124	103	0.83	0.7867	3.3	0.09721	1.5		0.44	**598**	8	589	15	556	65
CB55-55	2796	240	148	0.61	0.7680	7.5	0.08983	1.8		0.24	**555**	10	579	33	674	156
CB55-56	2216	222	239	1.08	0.6677	3.4	0.08547	0.6		0.18	**529**	3	519	14	478	74
CB55-57	3187	394	370	0.94	0.6561	2.6	0.08608	0.9		0.37	**532**	5	512	10	423	53
CB55-58	2167	107	131	1.22	7.0791	2.0	0.39167	0.4	-1	0.19	2131	7	2121	17	**2113**	34
CB55-60	1482	127	85	0.67	0.5892	3.7	0.07792	1.1		0.30	**484**	5	470	14	406	78
CB55-61	10304	94	45	0.48	5.5264	1.8	0.31354	1.1	15	0.62	1758	17	1905	16	**2068**	26
CB55-62	3626	417	319	0.77	0.5086	2.1	0.06871	0.4		0.17	**428**	1	417	7	358	47
CB55-63	3235	402	289	0.72	0.7177	2.6	0.08905	1.8		0.68	**550**	9	549	11	547	42
CB55-64	2930	628	53	0.09	0.6762	2.1	0.08333	1.4		0.70	**516**	7	524	8	562	32
CB55-65	5085	126	80	0.63	2.8429	2.2	0.24022	1.8	-4	0.79	1388	22	1367	17	**1334**	27
CB55-66	2145	100	46	0.45	1.1950	3.5	0.14167	1.8		0.50	**854**	14	798	19	646	66
CB55-67	1497	126	146	1.16	0.4867	7.3	0.06660	1.4		0.19	**416**	6	403	24	329	163
CB55-68	3068	271	309	1.14	0.8581	2.3	0.10189	0.7		0.32	**625**	4	629	11	642	48

Table 1. (Continued)

Grain spot	$^{206}Pb/^{204}Pb_c$	U ppm	Th ppm	$^{232}Th/^{238}U$	$^{207}Pb^*/^{235}U \pm 1\sigma$ %		$^{206}Pb^*/^{238}U \pm 1\sigma$ %		% disc	Err corr	Apparent ages					
											$^{206}Pb/^{238}U$ (Ma) $\pm1\sigma$		$^{207}Pb/^{235}U$ (Ma) $\pm1\sigma$		$^{207}Pb/^{206}Pb$ (Ma) $\pm1\sigma$	
(1)	(2)								(3)		(4)				(4)	
CB55-70	3085	105	113	1.07	0.6726	3.1	0.09343	1.0		0.32	**576**	5	522	13	294	68
CB55-71	1533	139	124	0.89	0.7139	6.1	0.08734	2.0		0.32	**540**	10	547	26	578	126
CB55-72	3154	108	169	1.57	0.7535	3.9	0.10312	1.5		0.39	**633**	9	570	17	329	82
CB55-74	7567	528	184	0.35	0.8436	1.5	0.10161	0.6		0.39	**624**	3	621	7	611	30
CB55-75	7769	395	509	1.29	0.8568	1.5	0.10352	0.9		0.63	**635**	6	628	7	604	25
CB55-76	4085	98	69	0.70	0.7116	5.1	0.08813	0.6		0.11	**544**	3	546	22	551	112
CB55-77	7254	159	47	0.29	1.7523	1.6	0.17385	0.6	-2	0.38	1033	6	1028	10	**1017**	30
CB55-78	4246	544	275	0.51	0.5364	2.3	0.07420	1.5		0.67	**461**	7	436	8	304	39
CB55-79	20779	290	256	0.88	13.8604	2.3	0.52280	2.2	2	0.98	2711	50	2740	22	**2762**	7
CB55-80	3895	60	24	0.39	2.4700	3.3	0.22352	0.6	-8	0.19	1300	7	1263	24	**1201**	64
CB55-82	4413	299	131	0.44	0.6732	2.5	0.08459	1.0		0.42	**523**	5	523	10	519	50
CB55-84	1379	201	105	0.52	0.4737	5.7	0.06641	1.4		0.24	**414**	6	394	18	274	126
CB55-85	8403	262	75	0.29	2.2838	2.1	0.19717	1.4	10	0.68	1160	15	1207	15	**1293**	30
CB55-86	2644	172	76	0.44	0.4693	5.6	0.06331	1.0		0.17	**396**	4	391	18	361	125
CB55-87	20149	353	118	0.33	1.3171	1.0	0.14002	0.4		0.43	**845**	3	853	6	875	18
CB55-88	3477	216	311	1.44	0.8278	5.3	0.09726	1.8		0.34	**598**	10	612	24	665	107
CB55-89	3418	98	64	0.66	0.6547	9.6	0.08280	0.9		0.10	**513**	5	511	39	505	212
CB55-90	3405	143	170	1.19	0.7086	3.4	0.09425	0.7		0.22	**581**	4	544	14	393	75
CB55-91	4855	58	36	0.63	2.0737	4.7	0.20371	0.8	-15	0.17	1195	9	1140	32	**1037**	94
CB55-92	13411	133	103	0.78	5.3820	0.8	0.33886	0.4	0	0.48	1881	6	1882	7	**1883**	13
CB55-93	690	13	47	3.59	1.5215	21.8	0.12165	2.6		0.12	**740**	18	939	137	1441	434
CB55-95	1072	50	37	0.75	0.9536	10.9	0.09783	2.4		0.22	**602**	14	680	54	949	221
CB55-96	2022	111	118	1.06	0.7409	4.3	0.09746	0.8		0.20	**600**	5	563	19	418	94
CB55-97	3587	76	54	0.71	1.1931	6.5	0.11929	4.4		0.67	**727**	30	797	36	1001	98
CB55-98	5112	79	60	0.75	2.7385	2.4	0.21812	0.4	12	0.15	1272	4	1339	18	**1448**	45
CB55-99	10159	311	220	0.71	0.8304	2.6	0.10113	1.1		0.41	**621**	6	614	12	587	51

(1): Sample identifier, spot number [missing numbers: spots were omitted due to high analytical errors]; (2): Isotope ratios corrected for common Pb using measured ^{204}Pb for correction. Individual errors are given as 1 sigma standard deviation; (3): Deviation of $^{206}Pb/^{238}U$ age relative to $^{207}Pb/^{206}Pb$ age is given only if $^{207}Pb/^{206}Pb$ age is considered as the most reliable apparent age. Positive values are for normal discordance, negative values for inverse discordance; (4): Most reliable apparent ages are in bold letters. Note: If the average of apparent ages is mid-Proterozoic and older (>900 Ma) then $^{207}Pb/^{206}Pb$ ages are considered as most reliable apparent ages; for younger values $^{206}Pb/^{238}U$ ages are used.

For a better comparison of the reliabilities between both methods, the individual errors are depicted in the diagrams (Figures 4-7) at the 2-σ level as it is common practice for LA-MC-ICPMS (*e.g.*, Dickinson and Gehrels, 2003).

Both analytical techniques (ion probe and LA-MC-ICPMS) are widely used for the determination of provenance ages of individual zircons (*e.g.*, DeGraaff-Surpless *et al.*, 2002; Dickinson and Gehrels, 2003; Weislogel *et al.*, 2006). The results and errors of both methods are similar for zircons that are not complex. The main difference, in practice, is the cost and the number of grains analyzed given that each ion probe analysis takes ~15 minutes whereas an analysis by LA-MC-ICPMS takes only ~90 seconds. For complex zircons, however, an ion probe is a more powerful tool because the excavation depth is <1 micron in comparison with 10–15 microns for laser ablation.

RESULTS

We analyzed zircons from two samples of fine-grained sandstone layers from the Upper Santa Rosa Formation close to Chicomuselo (Figure 3). Both samples have similar mineralogical compositions with 40–50% quartz, 20–30% altered feldspar, 10–15% altered oxides, 5–10% white mica, ~5% fresh plagioclase, and another 5% composed of chlorite, biotite, and heavy minerals like green tourmaline, zircon, titanite, and apatite. Matrix composed of sericite is rare. Clastic grains are principally quartz, plagioclase and altered feldspar. Occasionally, lithic fragments of very fine-grained quartzite could be observed (CB55). The clastic grains are little rounded, indicating, together with abundant detrital phyllosilicates, a nearby provenance of most of the detritus.

Zircons from sample CB55 were analyzed by LA-MC-ICPMS, and the data are listed in Table 1. Figure 4 shows a Concordia plot of all data (a) together with a relative probability plot (b) and a histogram plot (c). The oldest zircon analyzed has an apparent minimum $^{207}Pb/^{206}Pb$ age of 3.1 Ga, although its isotope ratios yield discordant ages. This grain and another almost concordant at 2.8 Ga indicate the presence of Archean zircons in the sample. A small group of four zircons represent a Paleoproterozoic population ($^{207}Pb/^{206}Pb$ ages = 2.0–2.16 Ga). One concordant grain is

Table 2. SHRIMP-RG U-Th-Pb data of detrital zircons from Santa Rosa sandstone sample SR1, Motozintla-Chicomuselo highway, Chiapas: long. -93.2306°, lat. 15.7172°.

Grain spot	$^{206}Pb_c$ %	U ppm	Th ppm	^{232}Th /^{238}U	$^{206}Pb^*$ ppm	$^{207}Pb^*/^{206}Pb^*$ ± 1σ %	$^{207}Pb^*/^{235}U$ ± 1σ %	$^{206}Pb^*/^{238}U$ ± 1σ %	% disc	Err corr	Apparent ages					
											$^{206}Pb/^{238}U$ (Ma) ± 1σ		$^{207}Pb/^{206}Pb$ (Ma) ± 1σ		$^{208}Pb/^{232}Th$ (Ma) ± 1σ	
(1)	(2)				(3)	(4)	(4)	(4)	(5)		(6)		(6)		(6)	
SR1-01	0.17	479	301	0.65	25.1	0.0539 2.6	0.452 3.3	0.0608 2		.622	**381**	8	366	58	388	11
SR1-02	0.41	256	110	0.44	14.8	0.0542 4.9	0.499 5.4	0.0667 2.2		.403	**416**	9	381	110	416	22
SR1-03	0.02	370	310	0.87	28.3	0.056 3.4	0.685 4	0.0888 2.1		.521	**548**	11	451	76	547	16
SR1-04	0.32	184	193	1.08	10.7	0.0531 5.6	0.492 6	0.0673 2.3		.373	**420**	9	331	130	408	15
SR1-05	--	236	8	0.04	32.9	0.0712 1.6	1.592 2.6	0.1623 2.1	-1	.795	969	19	**962**	33	1063	66
SR1-06	0.03	303	160	0.55	55.5	0.0817 1.3	2.401 2.5	0.2133 2.1	-1	.840	1246	23	**1237**	26	1239	35
SR1-07	0.42	89	56	0.66	6.77	0.0545 8.1	0.661 8.5	0.088 2.5		.292	**543**	13	390	180	496	33
SR1-08	0.33	471	438	0.96	38.7	0.0606 2.2	0.798 3	0.0955 2		.685	**588**	11	625	47	604	15
SR1-09	--	279	193	0.71	24	0.0603 2.2	0.833 3.1	0.1001 2.1		.685	**615**	12	615	48	630	24
SR1-10	0.23	410	47	0.12	22.6	0.0559 2.3	0.496 3.1	0.0643 2.1		.668	**402**	8	450	51	406	22
SR1-11	0.25	149	73	0.50	11.2	0.0603 2.8	0.725 3.6	0.0873 2.2		.616	**539**	12	613	61	598	34
SR1-12	0.17	441	278	0.65	36.6	0.0607 1.7	0.81 2.7	0.0967 2		.764	**595**	12	629	37	611	15
SR1-13	0.36	525	318	0.63	29.4	0.0572 2	0.514 2.9	0.0652 2.1		.719	**407**	8	498	44	413	11
SR1-14	0.04	64	34	0.55	4.79	0.0448 17	0.534 17	0.0864 2.7		.160	**534**	14	-66	410	419	60
SR1-15	0.69	59	73	1.28	7.57	0.0665 7.3	1.37 7.7	0.1491 2.6		.334	**896**	22	821	150	876	39
SR1-16	2.69	228	119	0.54	65.8	0.1318 1.2	6.09 2.4	0.3351 2.1	14	.869	1883	33	**2122**	21	1968	59
SR1-17	0.13	98	71	0.75	7.64	0.0487 11	0.601 12	0.0894 2.5		.213	**552**	13	135	270	496	36
SR1-18	0.17	150	50	0.35	12.9	0.0578 4.6	0.792 5.2	0.0994 2.3		.443	**611**	13	523	100	564	37
SR1-19	0.20	135	55	0.42	23.5	0.084 2.4	2.357 3.2	0.2035 2.2	8	.682	1194	24	**1292**	46	1302	51
SR1-20	0.16	95	37	0.40	19.2	0.088 2	2.839 3	0.2339 2.3	2	.762	1355	28	**1383**	37	1437	48
SR1-21	0.14	301	294	1.01	22.6	0.0594 2.2	0.717 3	0.0876 2.1		.698	**541**	11	582	47	543	14
SR1-22	0.74	972	1098	1.17	53	0.0528 5.5	0.458 5.8	0.0629 2		.347	**393**	7.7	322	120	385	11
SR1-23	0.25	66	33	0.52	9.29	0.0712 3.7	1.606 4.5	0.1635 2.5	-1	.563	976	23	**964**	75	965	44
SR1-24	--	553	505	0.95	44.3	0.0578 1.9	0.743 2.8	0.0933 2		.726	**575**	11	522	42	600	14
SR1-25	0.16	114	71	0.64	8.68	0.0555 5.2	0.673 5.7	0.088 2.3		.408	**544**	12	433	120	536	24
SR1-26	--	155	98	0.65	45.6	0.1155 1.1	5.45 2.4	0.3424 2.1	-1	.890	1898	35	**1887**	20	1918	48
SR1-27	--	283	618	2.26	21.6	0.0569 2.5	0.696 3.3	0.0888 2.1		.644	**548**	11	486	55	568	14
SR1-28	0.41	489	49	0.10	43.5	0.06375 1.5	0.91 2.6	0.1035 2.1		.800	**635**	12	733	33	585	35
SR1-29	0.21	92	74	0.83	6.99	0.0506 9	0.606 9.3	0.0869 2.4		.254	**537**	12	221	210	532	29
SR1-30	6.61	512	108	0.22	150	0.16275 0.6	7.61 2.1	0.3393 2	32	.956	1863	34	**2484**	10	1795	73
SR1-31	--	114	92	0.83	8.89	0.0569 3.8	0.713 4.4	0.0908 2.3		.519	**560**	12	489	83	557	19
SR1-32	0.76	106	158	1.55	7.71	0.0705 6.7	0.832 7.1	0.0857 2.4		.339	**530**	12	942	140	567	21
SR1-33	0.46	1241	440	0.37	61	0.0537 2.2	0.421 2.9	0.057 2		.673	**357**	7	357	49	335	12
SR1-34	--	93	67	0.75	8.04	0.0634 5.7	0.889 6.2	0.1016 2.4		.380	**624**	14	722	120	670	32
SR1-35	--	79	69	0.89	24.5	0.1202 1.4	5.95 2.7	0.3587 2.3	-1	.853	1976	39	**1960**	25	1946	53
SR1-36	2.73	570	140	0.25	236	0.18611 0.4	12.35 2	0.4814 2	7	.984	2533	41	**2708**	6	2538	67
SR1-37	--	84	55	0.67	18	0.0884 1.9	3.022 3	0.2478 2.3	-2	.760	1427	29	**1392**	37	1490	45
SR1-38	--	221	107	0.50	20.7	0.0623 2.7	0.943 3.5	0.1096 2.1		.614	**671**	14	686	58	729	25
SR1-39	3.55	407	158	0.40	49.4	0.0967 1.7	1.885 2.6	0.1413 2	83	.763	852	16	**1562**	32	828	23
SR1-40	0.23	224	139	0.64	18.1	0.0648 3.6	0.845 4.2	0.0945 2.2		.514	**582**	12	769	76	616	23
SR1-41	0.18	81	41	0.52	35.3	0.1791 1	12.49 2.5	0.506 2.3	0	.913	2638	49	**2645**	17	2580	74
SR1-42	0.18	483	328	0.70	39.7	0.06016 1.6	0.793 2.6	0.0956 2		.779	**588**	11	609	35	603	14
SR1-43	0.09	722	109	0.16	44.1	0.05615 1.5	0.55 2.5	0.0711 2		.800	**443**	8.6	458	34	456	15
SR1-44	--	86	66	0.79	7.56	0.0563 4.5	0.796 5.1	0.1026 2.4		.471	**629**	14	463	100	635	25
SR1-45	0.74	376	132	0.36	94.9	0.10763 0.8	4.362 2.2	0.2939 2	6	.936	1661	30	**1760**	14	1777	41
SR1-46	0.06	140	41	0.30	29.9	0.0899 1.6	3.086 2.8	0.2489 2.2	-1	.806	1433	29	**1424**	31	1404	51
SR1-47	0.31	631	357	0.58	205	0.13031 0.5	6.81 2	0.3788 2	2	.972	2071	35	**2102**	9	2087	43
SR1-48	2.19	728	347	0.49	109	0.0873 1.2	2.08 2.3	0.1728 2	33	.855	1028	19	**1367**	23	1052	27
SR1-49	1.14	153	123	0.83	44.9	0.1211 1.8	5.68 2.7	0.3404 2.1	4	.758	1889	34	**1972**	32	1820	51

(1): Sample identifier, spot number; (2): Contribution of common ^{206}Pb to total ^{206}Pb in %; (3): Concentration of radiogenic (*) lead ^{206}Pb; (4): Isotope ratios corrected for common Pb using measured ^{204}Pb for correction. Individual errors are given as 1 sigma standard deviation; (5): Deviation of $^{206}Pb/^{238}U$ age relative to $^{207}Pb/^{206}Pb$ age is given only if $^{207}Pb/^{206}Pb$ age is considered as most reliable apparent age. Positive values are for normal discordance, negative values for inverse discordance; (6); Apparent ages and all other corrections calculated with SQUID1.11 (Ludwig 2001). Most reliable apparent ages are in bold letters. Note: If the average of apparent ages is mid-Proterozoic and older (>900 Ma) then $^{207}Pb/^{206}Pb$ ages are considered as most reliable apparent ages, for younger values $^{206}Pb/^{238}U$ ages are used.
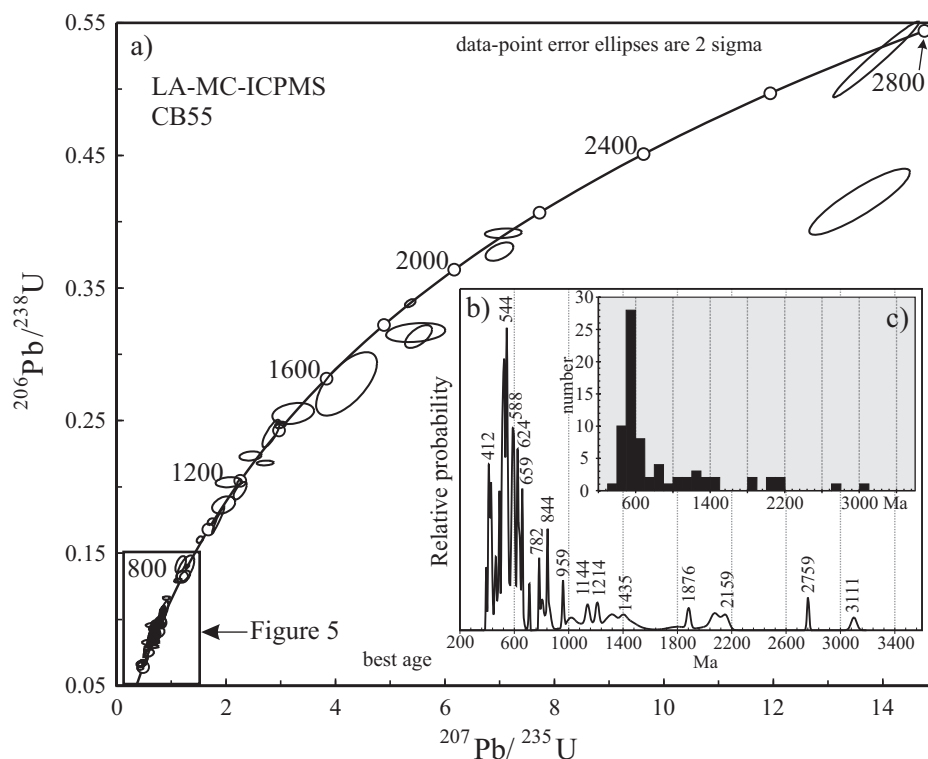
Figure 4. (a) Concordia diagram for U-Pb isotope ratios of zircons from sample CB55 measured by LA-MC-ICPMS. Error ellipses of individual spots are 2σ. (b) relative probability and (c) histogram plots of best ages for zircons analyzed. As best ages we defined $^{206}Pb/^{238}U$ apparent ages for average apparent ages <900 Ma and $^{207}Pb/^{206}Pb$ apparent ages for average apparent ages >900 Ma.

about 1.88 Ga old. The next small group of three zircons has ages of 1.4 to 1.6 Ga. Several fairly concordant zircons (eight grains) have $^{207}Pb/^{206}Pb$ apparent ages between 1.3 and 0.95 Ga, which can be grouped together with the Grenville-type zircons.

The great majority of zircons (about 75 %) are younger than Mesoproterozoic. A detailed concordia plot of these mostly concordant zircons together with weighted mean age calculations of prominent age groups is given in Figure 5. A small group of five early Neoproterozoic grains (group 5, Figure 5) yielded a mean $^{206}Pb/^{238}U$ age of 816 ± 47 Ma (2σ,). Isotopic ratios of 36 grains have apparent $^{206}Pb/^{238}U$ ages between 500 and 700 Ma, of which 28 are between 500 and 600 Ma (Figure 4c). From these zircons, three age groups were distinguished. A group of six grains yielded a mean $^{206}Pb/^{238}U$ age of 629.0 ± 9.6 Ma (2σ, group 4, Figure 5), a group of nine grains yielded a mean $^{206}Pb/^{238}U$ age of 544.7 ± 6.0 Ma (2σ, group 3, Figure 5), and another group of nine grains yielded a mean $^{206}Pb/^{238}U$ age of 521.0 ± 7.0 Ma (2σ, group 2, Figure 5). The youngest zircons (group 1, Figure 5) yielded a late Silurian mean $^{206}Pb/^{238}U$ age of 422.0 ± 12.4 Ma (2σ).

Zircons from sample SR01 were analyzed by SHRIMP, and the data are shown in Table 2. Figure 6 shows a concordia plot of all data (a) together with a relative probability plot (b) and a histogram plot (c). Three grains, of which two are nearly concordant and one discordant (Figure 6a),

are of late Archean age. A group of five grains have apparent $^{207}Pb/^{206}Pb$ ages between 1.9 and 2.1 Ga, and another measurement yielded a $^{207}Pb/^{206}Pb$ age of 1.76 Ga. Three concordant grains are about 1.4 Ga old, and another discordant zircon has a similar $^{207}Pb/^{206}Pb$ age. Each of the 1.2 to 1.3 Ga and the 0.95 to 1.0 Ga Grenville-type ages are represented by two concordant grains. About half of the analyzed spots yielded Pan-African-Brasiliano ages between 500 and 700 Ma. Two groups of concordant zircons yielded mean $^{206}Pb/^{238}U$ ages of 629 ± 21 Ma (2σ, group 3, Figure 6) and 558 ± 7 Ma (2σ, group 2, Figure 7). Another group of seven zircons (group 1, Figure 7) yielded a mean $^{206}Pb/^{238}U$ age of 416 ± 19 Ma (2σ).

DISCUSSION

The U-Pb zircon data presented here clearly show that the main source area of detrital components for the sandstone samples from the Upper Santa Rosa Formation at Chicomuselo is dominated by the Pan-African-Brasiliano orogenic cycle. This source includes rocks with ages of ~630 Ma, 540–560 Ma, ~520 Ma and, in a broader sense, also a less pronounced population of ~820 Ma. There are no outcrops of igneous and metamorphic rocks of any of those ages known from Mexico and Central America that may be considered as the local source of sediments for
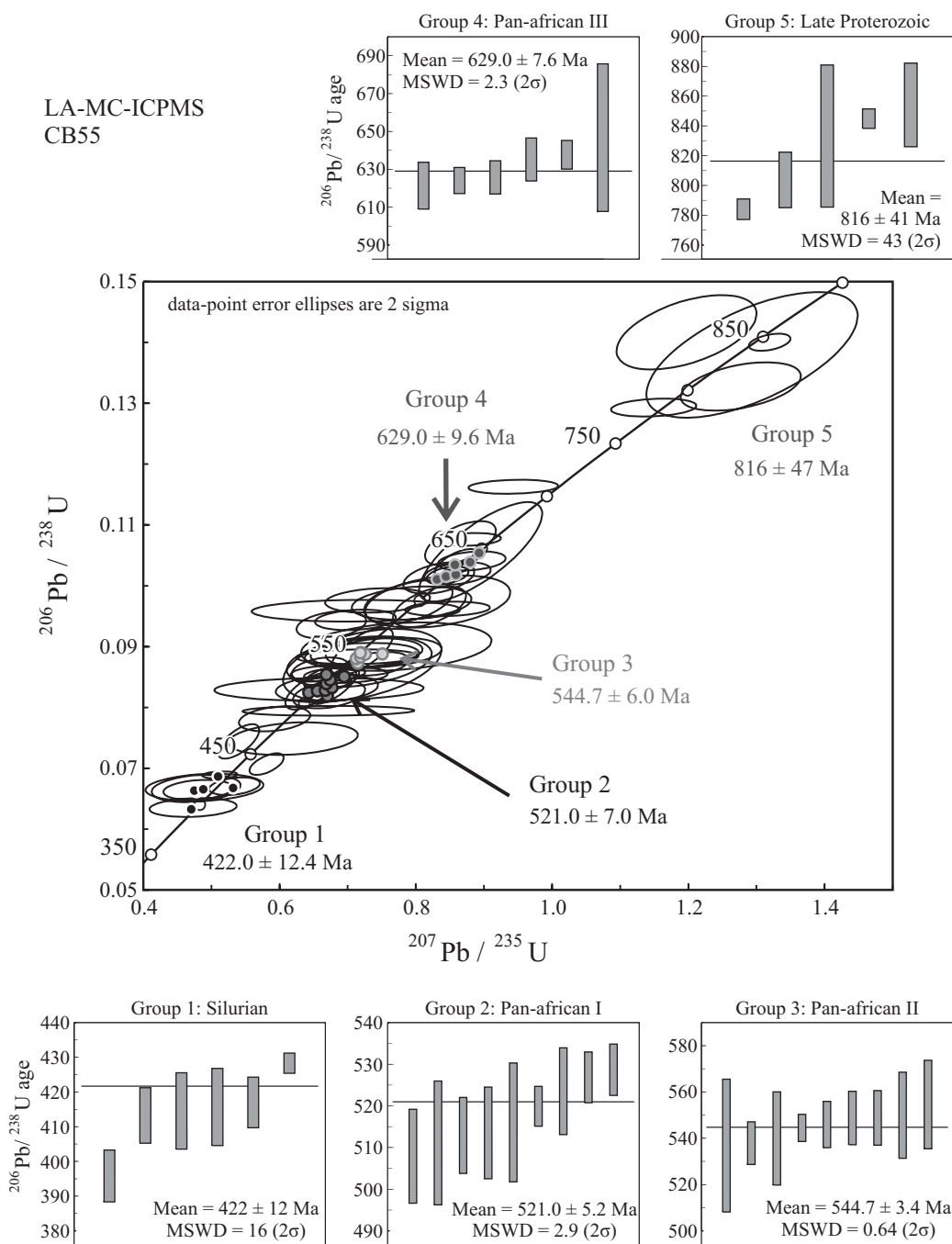
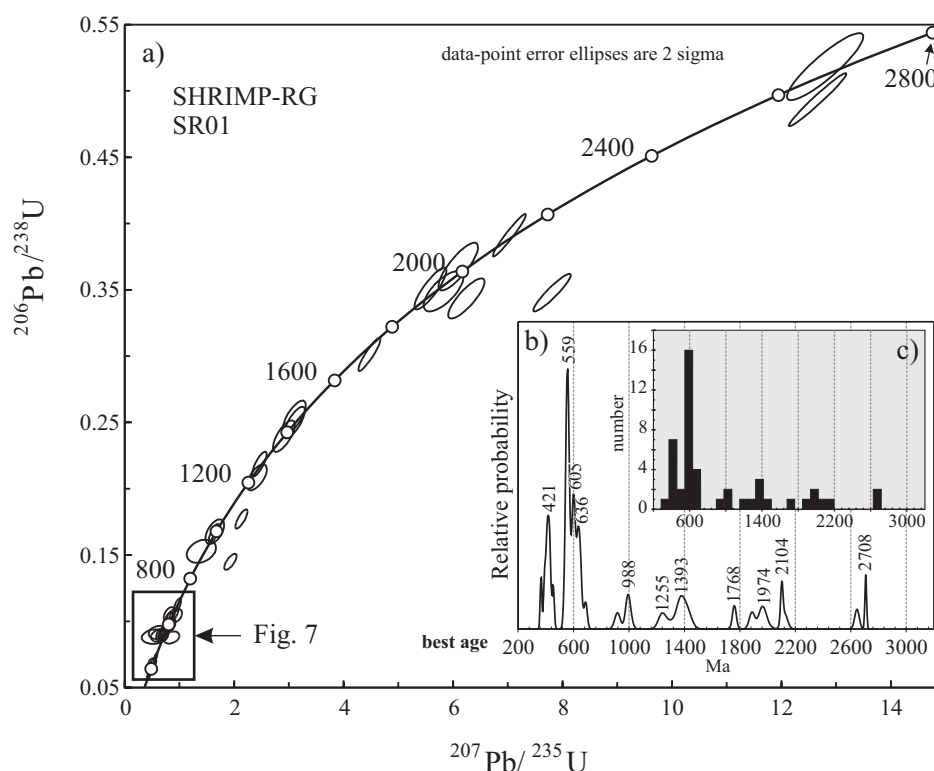Figure 5. Lower part of concordia diagram for U-Pb isotope ratios of zircons from sample CB55 measured by LA-MC-ICPMS. Error ellipses of individual spots are 2σ. Mean ^{206}Pb/^{238}U ages calculated from the respective group of spots marked by filled dots in the Concordia diagram include a systematic error of 0.9% and are given at 2σ level. 2σ error bars of ^{206}Pb/^{238}U apparent ages of individual spots and weighted means calculated from zircon populations "Group 1" to "Group 5" without systematic error.

the Upper Santa Rosa Formation. However, Krogh *et al.* (1993) reported an average age of 545 ± 5 Ma for shocked zircons from ejecta of the Chicxulub impact structure of northwestern Yucatán, and Lopez *et al.* (2001) obtained a 580 ± 4 Ma concordant zircon age from granitic boulders within sediments of the Mexican state of Coahuila. Therefore, detrital zircons from the Pan-African-Brasiliano

orogenic cycle are not uncommon in the Maya block and probably occur in similar Paleozoic sediments of eastern and northeastern Mexico.

It is widely accepted that, after fragmentation of Rodinia in the early Neoproterozoic, Western Gondwana was assembled by diachronous convergence and collision of several cratonic landmasses which lasted from 650 to

Figure 6. (a) Concordia diagram for U-Pb isotope ratios of zircons from sample SR01 measured by SHRIMP-RG. Error ellipses of individual spots are 2σ. (b) relative probability and (c) histogram plots of best ages for zircons analyzed. As best ages we defined $^{206}Pb/^{238}U$ apparent ages for average apparent ages <900 Ma and $^{207}Pb/^{206}Pb$ apparent ages for average apparent ages >900 Ma.

500 Ma (*e.g.*, Veevers, 2003). Circum-cratonic convergence and collision of the West African craton started in the Bassarides-Mauritanides (BA, Figure 8) of present-day West Africa at 665–655 Ma, progressing clockwise around the craton, arriving at the Brasiliano belt (BR, Figure 8) at 600–550 Ma, and finally at the Rokelides (R, Figure 8) with ages from 547–500 Ma in West Africa (*e.g.*, Doblas *et al.*, 2002) and Florida (*e.g.*, Hatcher, 2002). The Brazilide Ocean was closed at 650–600 Ma, followed by intracontinental convergence that culminanted at ~550 Ma during the final assemblage of Western Gondwanaland (*e.g.*, Alkmin *et al.*, 2001). Taking into consideration these models, the most probable source regions for the Pan-African-Brasiliano zircons of the Upper Santa Rosa Formation are West Africa and northeastern South America. Archean (2.6–3.1 Ga) zircons and more abundant Paleoproterozoic (1.8–2.2 Ga) populations probably came either from the northern Amazonian or West African cratons, indicating similar source regions as for the Pan-African-Brasiliano zircons. In Florida, detrital zircons from a subsurface sandstone sample have main age populations of (1) 515 to 637 Ma and (2) 1.9 to 2.3 Ga (Mueller *et al.*, 1994), indistinguishable from our present zircon age data and indicating a similar provenance for the Florida sedimentary basement and the Upper Santa Rosa Formation.

Zircons of Mesoproterozoic (1.4–1.6) and Grenville (0.95–1.3 Ga) ages must be from a different source, as there is little or no record of those ages from eastern South America and West Africa. These zircons, although the populations are of minor importance, may either come from one of the terranes with Grenville affinity, namely Oaxaquia and the Colombian or Venezuelan terranes where such ages are common (Restrepo-Pace *et al.*, 1997; Aleman and Ramos, 2000), or they come from eastern Laurentia. The youngest zircon population from the Upper Santa Rosa Formation is of Silurian age (~420 Ma). Granite intrusions of this age are exposed in the southern Maya block in the Maya Mountains of Belize (Figure 1; Steiner and Walker, 1996). These intrusive rocks were either already exposed to erosion in the late Carboniferous, or the zircons came from contemporaneous felsic volcanic rocks which can be observed as boulders in some of the conglomerate layers of the Santa Rosa Formation.

The provenance ages of the Upper Santa Rosa Formation support a model in which the Maya block, together with other terranes with similar late Paleozoic flysch-type sedimentary rocks, like the Delicias Basin in Coahuila, Mexico (McKee *et al.*, 1999), Florida, and the Mérida terrane of Venezuela (Alemán and Ramos, 2000), were located at the northwestern Gondwana margin during the late Carboniferous (Figure 8). By closing the Theic Ocean, Gondwana collided with Laurentia during
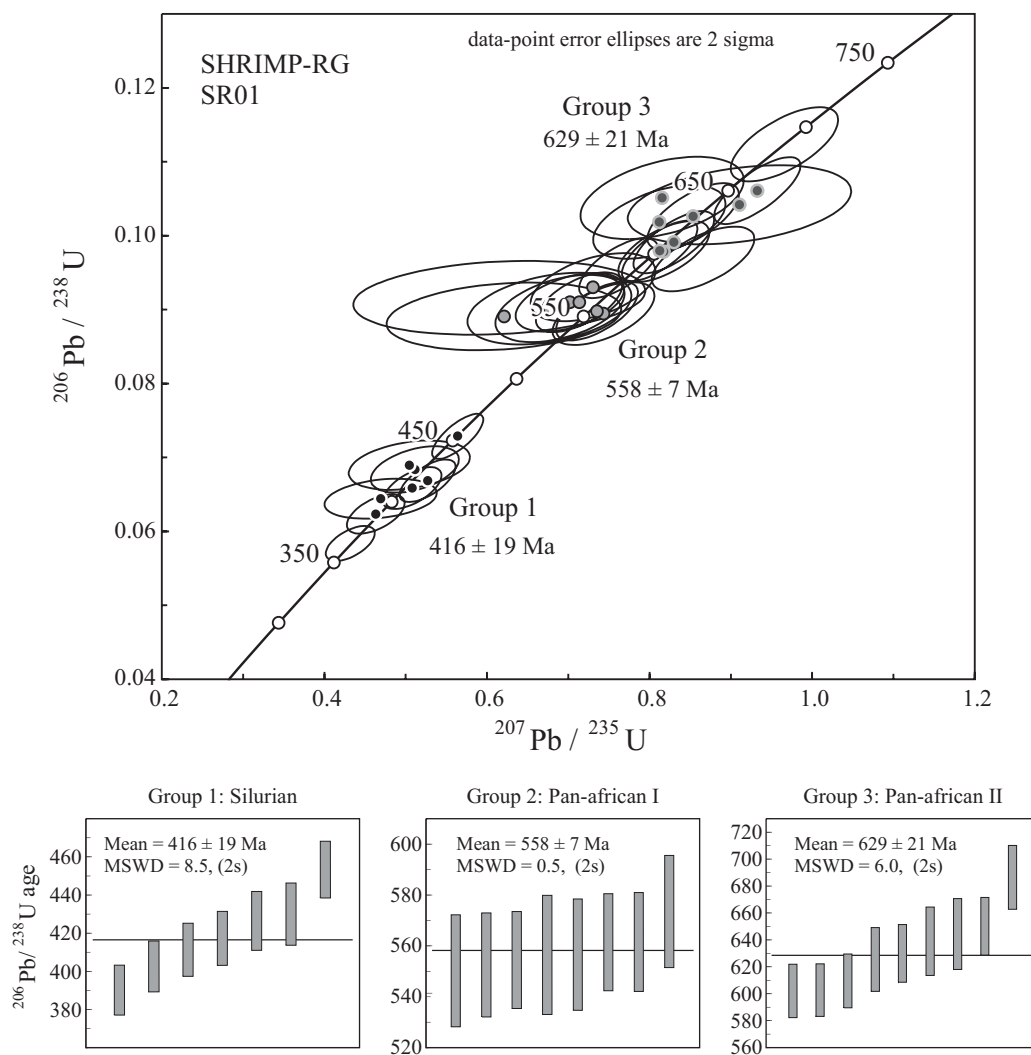
Figure 7. Lower part of concordia diagram for U-Pb isotope ratios of zircons from sample SR01 measured by SHRIMP. Error ellipses of individual spots are 2σ. Mean $^{206}Pb/^{238}U$ ages calculated from the respective group of spots marked by filled dots. 2σ error bars of $^{206}Pb/^{238}U$ apparent ages of individual spots and weighted mean age calculated from zircon populations "Group 1" to "Group 3".

the Alleghanian orogeny. This orogeny lasted from 320 to 280 Ma, starting in the northern Appalachians and ending in the Marathon-Ouachita belt. Hatcher (2002) explained the diachronous closure of the former Theic ocean and the Alleghanian orogeny by so-called "zipper tectonics" which means rotational (clockwise) transpressive continent-continent collision. Zipper closing started in the present northwest, inducing dextral srike-slip deformation in the southern and central Appalachians.

On the basis of this hypothesis, our new zircon data, and previous paleogeographic reconstructions (Rowley and Pindell, 1989; Dickinson and Lawton, 2001; Elías-Herrera and Ortega-Gutiérrez, 2002) we suggest the following model (Figure 8): 1) During the late Carboniferous (deposition of the Upper Santa Rosa Formation), the Maya block together with Florida and other supracrustal blocks was located close to West Africa or northeastern South America, defined as

Gondwana margin or Perigondwanan terranes; 2) most of the flysch-type sedimentation occurred southwestward by erosion of the newly formed mountain chains of the early Alleghanian orogen; (3) ongoing zipper tectonics towards the southwest caused dextral strike-slip movement south of the future Ouachita-suture and westward movement of the Maya block, probably together with other similar crustal blocks, and attached oceanic lithosphere. The accommodation of these blocks and Grenville-type basement terranes, especially Oaxaquia, at the western margin of the newly formed Pangea supercontinent, together with initiating subduction and arc-magmatism along the western margin of former Gondwana, stopped sedimentation and westward movement of the Maya block. This is documented by deformation, metamorphism, and magmatism during the Permian in the southern Maya block, namely in the Chiapas Massif (Weber *et al.*, 2005, 2006).
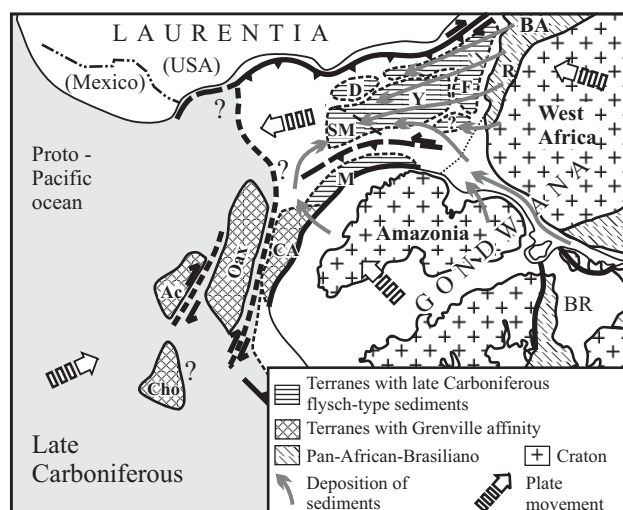
Figure 8. Late Carboniferous geotectonic reconstruction of west-central Pangea, showing Proterozoic and Paleozoic crystalline blocks of Mexico and Central America and northern South America modified after Elías-Herrera and Ortega Gutiérrez (2002) and Dickinson and Lawton (2001), with special emphasis on the position of the Maya block and other terranes with Late Paleozoic flysch-type sediments. Grey arrows indicate the probable sediment transport directions. Abbreviations are Ac: Acatlan Complex; BA: Bassarides-Mauritanides; BR: Brasiliano belts; Chis: Chiapas Massif protoliths; Cho: Chortís block; CA: Colombian Andes; D: Delicias basin; F, Florida; M: Mérida terrane; SM: Southern Maya block; R: Rokelides; Y: Yucatán.

ACKNOWLEDGEMENTS

REFERENCES

Aleman, A., Ramos, V.A., 2000, Northern Andes, *in* Cordani, U.G., Milani, E.J., Thomaz Filho, A., Campos, D.A. (eds.), Tectonic Evolution of South America: Rio de Janeiro, 31st International Geological Congress, Servicio Geológico de Brazil (SGB), Companhia de Pesquisa de Recursos Minerais (CPRM), 453-480.

Alkmin F.F., Marshak, S., Fonseca, M.A., 2001: Assembling West Gondwana in the Neoproterozoic: Clues from the São Francisco craton region, Brazil: Geology, 29(4), 319-322.

Anderson, T.H., Schmidt, V.A., 1983, The evolution of Middle America and the Gulf of Mexico - Caribbean Sea region during Mesozoic time: Geological Society of America Bulletin, 94(8), 941-966.

Bateson, J.H., Hall, I.H.S., 1977, The Geology of the Maya Mountains, Belize: London, Institute of Geological Science, Her Majesty´s Stationery Office, Overseas Memoir 3, 43 p.

Black, L.P., Kamo, S.L., Allen, C.M., Davis, D.W., Aleinikoff, J.N., Valley, J.W., Mundil, R., Campbell, I.H., Korsch, R.J., Williams, I.S., Foudoulis, C., 2004, Improved $^{206}Pb/^{238}U$ microprobe geochronology by the monitoring of a trace-element-related matrix effect; SHRIMP, ID–TIMS, ELA–ICP–MS and oxygen isotope documentation for a series of zircon standards: Chemical Geology, 205, 115-140.

Bullard, Sir, E., Everett, J.E., Smith, A.G., 1965, The fit of the continents around the Atlantic: Philosophical Transactions of the Royal Society of London, A, 258, 41-51.

Burkart, B., 1983, Neogene North American-Caribbean plate boundary across Northern Central America; Offset along the Polochic Fault: Tectonophysics, 99, 251-270.

Burkart, B., Self, S., 1985, Extension and rotation of crustal blocks in northern Central America and effect on the volcanic arc: Geology, 13, 22-26.

Campa, M.F., Coney, P.J., 1983, Tectono-stratigraphic terranes and mineral resource distributions in México: Canadian Journal of Earth Sciences, 20, 1040-1051.

Clemons R.E., 1966, Geology of the Chiquimula Quadrangle, Guatemala: Austin, University of Texas, Ph. D. thesis (unpublished).

Clemons, R.E., Burkart, B., 1971, Stratigraphy of northwestern Guatemala: Boletín de la Sociedad Geológica Mexicana, 32(2), 143-158.

Damon, P.E., Shafiqullah, M., Clark, K., 1981, Age trends of igneous activity in relation to metallogenesis in the southern Cordillera, *in* Dickinson, W., Payne, W.D. (eds), Relations of Tectonics to Ore Deposits in the Southern Cordillera: Tucson, AZ, Arizona Geological Society Digest, 14, 137-153.

DeGraaff-Surpless, K., Wooden, J.L., McWilliams, M.O., 2002, Detrital zircon provenance analysis of the Great Valley Group, California; Evolution of an arc-forearc system: Geological Society of America Bulletin, 114, 1564-1580.

Dengo, G., 1985, Mid America; Tectonic setting for the Pacific margin from southern México to northwestern Colombia, *in* Nairn, A.E.M., Stehli, F.G. (eds.), The Oceanic Basins and Margins, vol. 7a, The Pacific Ocean: New York, Plenum Press, 123-180.

Dickinson, W.R., Gehrels, G.E., 2003, U–Pb ages of detrital zircons from Permian and Jurassic eolian sandstones of the Colorado Plateau, USA; paleogeographic implications: Sedimentary Geology, 163, 29-66.

Dickinson, W.R., Lawton, T.F., 2001, Carboniferous to Cretaceous assembly and fragmentation of México: Geological Society of America Bulletin, 113, 1142-1160.

Dixon, C.G., 1956, Geology of southern British Honduras with notes on adjacent areas: Belize, Gobernment Printer, 85 p.

Doblas, M., López-Ruiz, J., Cebriá, J.M., Youbi, N., Degroote, E., 2002, Mantle insulation beneath the West African craton during the Precambrian-Cambrian transition: Geology, 30(9), 839-842.

Dollfus, A., Montserrat, E., 1868, Voyage géologique dans les Républiques de Guatemala et de Salvador, Mission scientifique au Mexique et dans l'Amerique centrale, Géologie: Paris, Imprimerie Impériale, 539 pp.

Donelly, T.W., Horne, G.S., Finch, R.C., López- Ramos, E., 1990, Northern Central America; the Maya and Chortís blocks, *in* Dengo, G., Case, J.E. (eds.), Decade of North American Geology, Volume H, The Caribbean Region: Boulder, Geological Society of America, 37-76.

Elías-Herrera, M., Ortega-Gutiérrez, F., 2002, Caltepec fault zone; An early Permian dextral transpressional boundary between the Proterozoic Oaxacan and Paleozoic Acatlán complexes, southern México, and regional tectonic implications: Tectonics, 21, 1-19.

French, C.D., Schenk, C.J., 1997, Map showing geology, oil and gas fields, and Geologic Provinces of the Caribbean Region (CD-ROM): Denver, United States Geological Survey, Open File Report 97-470-K.

Hatcher, R.D., 2002, Alleghanian (Appalachian) orogeny, a product of zipper tectonics; Rotational transpressive continent-continent

collision and closing of ancient oceans along irregular margins, *in* Martínez-Catalán, J.R., Hatcher, R.D., Arenas, R., Díaz-García, F. (eds), Variscan-Appalachian Dynamics; The building of the late Paleozoic basement: Boulder, Colorado, Geological Society of America, Special Paper, 364, 199-208.

Hernández-García, R., 1973, Paleogeografía del Paleozoico de Chiapas, México: Boletín de la Asociación Mexicana de Geólogos Petroleros, 25, 79-113.

Hiller, R., Weber, B., Hecht, L., Ortega-Gutiérrez, F., Schaaf, P., López-Martínez, M., 2004, The Sepultura unit – A médium to high grade metasedimentary sequence in the Chiapas Massif, SE México (abstract), *in* IV Reunión Nacional de Ciencias de la Tierra, Querétaro, México, Libro de Resumenes: Sociedad Geológica Mexicana, p. 200.

Jiménez-Hernández, A., Jaimez-Fuentes, A., Motolinía-García, O., Pinzón-Salazar, T., Membrillo-Ortega, H., 2005, Carta Geológica-Minera Huixtla D15-2 Chiapas, 1:250,000: Pachuca, Hgo., Servicio Geológico Mexicano, 1 map.

Krogh, T.E., Kamo, S.L., Sharpton, V.L., Martin, L.E., Hildebrand, A.R., 1993, U-Pb ages of single shocked zircons linking distal K/T ejecta to the Chicxulub crater: Nature, 366, 731-734.

Lopez, R., Cameron, K.L., Jones, N.W., 2001, Evidence for Paleoproterozoic, Grenvillian, and Pan-African age crust beneath northeastern México: Precambrian Research, 107, 195-214.

López-Ramos, E., 1979, Geología de México, Tomo III: México D.F., 446 pp.

Ludwig, K.R., 2001, Users manual for SQUID version 1.02: Berkeley Geochronology Center, Special Publication 2, 19 p.

Ludwig, K.R., 2003, ISOPLOT; A geochronological toolkit for Microsoft Excel, Version 3.00: Berkeley Geochronology Center, Special publication, 4, 70 p.

McKee, J.W., Norris, W.J., Anderson, T.H., 1999, Late Paleozoic and early Mesozoic history of the Las Delicias terrane, Coahuila, Mexico: Geological Society of America, Special Paper, 340, 161-189.

Muehlberger, W.R., Ritchie, A.W., 1975, Caribbean-Americas plate boundary in Guatemala and southern Mexico as seen on Skylab IV orbital photography: Geology, 3(5), 232-235.

Mueller, P.A., Heatherington, A.L., Wooden, J.L., Shuster, R.D., Nutman, A.P., Williams, I.S., 1994, Precambrian zircons from Florida basement; A Gondwanan connection: Geology, 22(2), 119-122.

Nourse, J.A., Premo, W.R., Iriondo, A., Stahl, E.R., 2005, Contrasting Proterozoic basement complexes near the truncated margin of Laurentia, northwestern Sonora-Arizona international border region, *in* Anderson, T.H., Nourse, J.A., McKee, J.W, Steiner, M.B. (eds.), The Mojave-Sonora Megashear Hypothesis: Development, Assessment, and Alternatives: Boulder, Colorado, Geological Society of America, Special Paper, 393, 123-182.

Ortega-Gutiérrez, F., Mitre-Salazar, L.M., Roldán-Quintana, J., Aranda-Gómez, J.J., Morán-Zenteno, D., Alaniz-Álvarez, S.A., Nieto-Samaniego, A.N., 1992, Carta geológica de la República Mexicana 1:2,000,000: México, D.F., Universidad Nacional Autónoma de México, Instituto de Geología, 1 map.

Ortega-Gutiérrez, F., Sedlock, R.L., Speed, R.C., 1994, Phanerozoic tectonic evolution of Mexico, *in* Speed, R.C. (ed.), Phanerozoic evolution of North American continent-ocean transitions: Geological Society of America, DNAG Continental-Ocean Transect Volume, 265-306.

Ortega-Gutiérrez, F., Ruiz, J., Centeno-García, E., 1995, Oaxaquia, a Proterozoic microcontinent accreted to North America during the late Paleozoic: Geology, 23, 1127-1130

Ortega-Gutiérrez, F., Solari, L., Ortega-Obregón, 2004, Tectonostratigraphic análisis at the southern margin of the Maya Block; where is the limit? (abstract), *in* IV Reunión Nacional de Ciencias de la Tierra, Querétaro, México, Libro de Resumenes: Sociedad Geológica Mexicana, p. 204.

Pindell, J.L., Barrett, S.F., 1990, Geological evolution of the Caribbean region; A plate-tectonic perspective, *in* Dengo, G., Case, J.E. (eds.), Decade of North American Geology, Volume H, The Caribbean Region: Boulder, Geological Society of America, 405-432.

Pindell, J.L., Kennan, L., Barrett, S., 2000, Putting it all together again: American Association of Petroleum Geologists, Explorer, 21, 34-37.

Restrepo-Pace, P.A., Ruíz, J. Gehrels, G., Cosca, M., 1997, Geochronology and Nd isotopic data of Grenville-age rocks in the Colombian Andes; new constraints for Late Proterozoic-Early Paleozoic paleocontinental reconstructions of the Americas: Earth and Planetary Science Letters, 150, 427-441.

Roberts, R.J., Irving, E.M., 1957, Mineral deposits of Central America: United States Geological Survey, Bulletin, 1034, 205 p.

Ross, M.I., Scotese, C.R., 1988, A hierarchical tectonic model of the Gulf of Mexico and Caribbean region, *in* Scotese, C.R., Sager, W.W. (eds.), Mesozoic and Cenozoic Plate Reconstructions: Tectonophysics, 155, 139-168.

Rowley, D.B., Pindell, J.L., 1989, End Paleozoic - early Mesocoic estern Pangean reconstruction and its implications for the distribution of Precambrian and Paleocoic rocks around Meso-America: Precambrian Research, 42, 411-444.

Sapper, K., 1937, Mittelamerika; Handbuch der regionalen Geologie, Band 8, Abt. 4a, Heft 29: Heidelberg, Carl Winter, 160 pp.

Schaaf, P., Weber, B., Weis, P., Groß, A., Ortega-Gutiérrez, F., Köhler, H., 2002, The Chiapas Massif (México) revised; New geologic and isotopic data for basement characteristics, *in* Miller, H. (ed), Contributions to Latin-American Geology: Neues Jahrbuch für Geologie und Paläontologie, Abhandlungen, 225, 1-23

Sedlock, R.L., Ortega-Gutiérrez, F., Speed, R.C., 1993, Tectonostratigraphic terranes and tectonic evolution of Mexico: Boulder Colorado Geological Society of America, Special Paper, 278, 153 p.

Shurbet, D.H., Cebull, S.E., 1984, Tectonic interpretation of the Trans-Mexican volcanic belt: Tectonophysics, 101, 159-165,

Stacey, J.S.K., Kramers, J.D., 1975, Approximation of terrestrial lead isotope evolution by a two-stage model: Earth and Planetary Science Letters, 26, 2, 207-221.

Steiner, M.B., Walker, J.D., 1996, Late Silurian Plutons in Yucatan: Journal of Geofisical Research, 101, 17727-17735.

Torres, R., Ruiz, J., Patchett, P.J., Grajales, J.M., 1999, Permo-Triassic continental arc in eastern México; Tectonic implications for reconstructions of southern North America: Boulder Colorado, Geological Society of America, Special Paper, 340, 191-196.

Veevers, J.J., 2003. Pan-African is Pan-Gondwanaland; Oblique convergence drives rotation during 650–500 Ma assembly: Geology, 31(6), 501-504.

Vinson, G.L., 1962, Upper Cretaceous and Tertiary stratigraphy of Guatemala: Bulletin of the American Association of Petroleum Geologists, 46, 425-456.

Walper, J.L., 1960, Geology of Coban-Purulha area, Alta Verapaz, Guatemala: Bulletin of the American Association of Petroleum Geologists, 42, 1273-1315.

Weber, B., Gruner, B., Hecht, L., Molina-Garza, R.S., Köhler, H., 2002, El descubrimiento de basamento metasedimentario en el macizo de Chiapas; la "Unidad La Sepultura": Geos, 22, 2-11.

Weber, B., Cameron, K.L., Osorio, M., Schaaf, P., 2005, A late Permian tectonothermal event in Grenville crust of the Southern Maya terrane; U-Pb zircon ages from the Chiapas massif, Southeastern México: International Geology Review, 47, 509-529.

Weber, B., Iriondo, A., Premo, W.R., Hecht, L., Schaaf, P., 2006, New insights into the history and origin of the southern Maya Block, SE México; U-Pb-SHRIMP zircon geochronology from metamorphic rocks of the Chiapas Massif: International Journal of Earth Sciences (Geologische Rundschau), DOI 10.1007/s00531-006-0093-7.

Weislogel., A.L., Graham, S.A., Chang, E.Z., Gehrels, G.E., Yang., H., 2006, Detrital zircon provenance of the Late Triassic Songpan-Ganzi complex; Sedimentary record of the North and South China blocks: Geology, 34, 97-100.